



**HAL**  
open science

## Covering a Surface with Pre-stressed Ribbons: From Theory to Nano-Structures Fabrication

Alexandre Danescu, Philippe Regreny, Pierre Cremillieu, Jean -Louis Leclercq,  
Ioan Ionescu

► **To cite this version:**

Alexandre Danescu, Philippe Regreny, Pierre Cremillieu, Jean -Louis Leclercq, Ioan Ionescu. Covering a Surface with Pre-stressed Ribbons: From Theory to Nano-Structures Fabrication. Theoretical Analyses, Computations, and Experiments of Multiscale Materials, 175, Springer International Publishing, pp.671-687, 2022, Advanced Structured Materials, 10.1007/978-3-031-04548-6\_31 . hal-04137691

**HAL Id: hal-04137691**

**<https://ec-lyon.hal.science/hal-04137691>**

Submitted on 26 Jan 2024

**HAL** is a multi-disciplinary open access archive for the deposit and dissemination of scientific research documents, whether they are published or not. The documents may come from teaching and research institutions in France or abroad, or from public or private research centers.

L'archive ouverte pluridisciplinaire **HAL**, est destinée au dépôt et à la diffusion de documents scientifiques de niveau recherche, publiés ou non, émanant des établissements d'enseignement et de recherche français ou étrangers, des laboratoires publics ou privés.

# Chapter 1

## Covering a surface with pre-stressed ribbons: from theory to nano-structures fabrication

Alexandre Danescu, Philippe Regreny, Pierre Cremillieu, Jean-Louis Leclercq, and  
Ioan R. Ionescu

**Abstract** The paper deals with the fabrication of nano-shells from pre-stressed nano-plates release. Due to geometrical and technological restrictions we have to cover a given surface with three-dimensional thin ribbons. We discuss the key role of the geodesic curvature in the design of such shell-ribbons. We show that including small-strains but large rotations we are able to control the metric tensor of both Lagrangian and Eulerian ribbons by an appropriate choice of the width and thickness of the ribbons. Moreover, the Green-Lagrange strain tensor is controlled by the distance between the curvature of the planar ribbon and the geodesic curvature of the supporting curve of the shell-ribbon. Under suitable constitutive assumptions, we deduce the field equations, the boundary conditions and the design equations. The former relate the pre-stress in the planar layer to the final geometry of the desired shell-ribbon. A fine tuning of the composition, geometry and of the pre-stress of the plate-ribbon is necessary to design and fabricate the shell-ribbon. We design and fabricate a partial cover of the sphere with constant latitude ribbons starting from planar multi-layer semiconductor materials grown by molecular beam epitaxy. The details of fabrication method and its limitations are discussed in detail.

**Keywords:** nonlinear elasticity, pre-stressed structures, shell-design, nano-structures, fabrication, epitaxial thin films

---

A. Danescu, Ph. Regreny, P. Cremillieu and Jean-Louis Leclercq  
Univ Lyon, Ecole Centrale de Lyon, CNRS, INSA Lyon, University Claude Bernard Lyon 1, CPE  
Lyon, CNRS, INL, UMR5270, 69130 Ecully, France  
e-mail: alexandre.danescu@ec-lyon.fr, philippe.regreny@ec-lyon.fr,  
pierre.cremillieu@ec-lyon.fr, jean-louis.leclercq@ec-lyon.fr

Ioan R. Ionescu  
LSPM, University Sorbonne-Paris-Nord, 93430 Villetaneuse, France and IMAR, Romanian  
Academy, Bucharest, Romania  
e-mail: ioan.r.ionescu@gmail.com

## 1.1 Introduction

Nowadays the fabrication processes in semiconductor industry use essentially the planar technology and among the various methods of crystal growth, the molecular beam epitaxy (MBE) presents the significant advantage of highly accurate control of composition (up to 1%) and thickness (up to monolayer). Composition control endow multi-layered planar structures with pre-stress which may be beneficial for the design on 3D objects by pre-stress relaxation. The prototype of this phenomena is the bi-layer material where the presence of the pre-stress in one of the layers induced the bending of the free bi-layer structure. Initiated in Prinz et al (2000) (see also Prinz et al (2001), Prinz (2003), Seleznev et al (2003), Prinz and Golod (2006), Prinz et al (2017)) for simple rolls, curls and developable ribbons the method was extended to cover more complex situations in Danescu et al (2013), Danescu et al (2018). Introduced by an heuristic method in Danescu et al (2013) and later reconsidered in the framework of small-strains and large-rotations in Danescu and Ionescu (2021), the geodesic curvature represents the key concept for the design of 3D structures from planar pre-stresses films. From a different point of view, the equilibrium shape of a pre-stressed material was investigated by using dimension reduction in Le Dret and Raoult (1995); Friesecke et al (2002a,b, 2006); de Benito Delgado and Schmidt (2020); Wang et al (2019); de Benito Delgado, Miguel and Schmidt, Bernd (2021) leading to a hierarchy of non-linear elastic models Lewicka and Raoult (2018).

These previous results concerning relaxation of pre-stressed bi-layer materials focus on straight ribbons that relax toward rolls and curls, all based on isometric transformations. However, it is well-known that the class of isometries between planar and three-dimensional surfaces, extensively studied in Fosdick and Fried (2016), is too narrow to cover simple non-developable surfaces occurring in pre-stressed relaxation design problems. To circumvent this theoretical drawback, in a recent paper Danescu and Ionescu (2020) we developed a shell design model built on a non-isometric perturbation assumption of Love-Kirchhoff type superposed on a plate-to-shell theory. Extending shell models in Steigmann (2013), Ciarlet and Mardare (2018), Steigmann (2007b), Steigmann (2007a), Steigmann and Ogden (2014)) the geometric description involves a single small parameter  $\delta \ll 1$ , the product between the thickness of the shell and its curvature.

The main difficulty in applying the shell-design model in Danescu and Ionescu (2020) is of a geometric nature. Indeed, for several common mid-surfaces the small-strain assumption drastically reduces the surface width. However, since we are focusing on brittle-elastic materials (such as semiconductors), the small deformations assumption is merely a technological restriction and not a mathematical simplification. To encompass this limitation, in Danescu and Ionescu (2021) another type of shell, (called a strip-shell) is constructed, for which this assumption can be fulfilled by an appropriate choice of an additional geometric parameter, namely the strip width. In this restricted framework, if the product between the strip-shell width and its curvature is of order  $\delta^{1/2}$  the assumptions of plate-to-shell theory Danescu and Ionescu (2020) are fulfilled so that, for any strip of a given shell we provide a simple model able to design the corresponding plate-strip (i.e., to compute the shape

and pre-stress momentum of the plate). The next step analysed here is to cover the given surface (shell) with one or several strips, situation in which we can provide an explicit design of the corresponding planar (plate) strips.

The paper is organized as follows : the first two sections recall the geometric and mechanical assumptions of the plate to shell model for design proposed in Danescu and Ionescu (2020). We relate the geometric aspects to the pre-stress via constitutive relations and field equations in finite strains through the assumption of weak-transversal heterogeneity, assumption fulfilled here by the weak variation of the composition in our crystal growth process. The third section discuss the main geometric aspects of the theory (see Danescu and Ionescu (2021) for more details), with a particular accent on the metric tensors for planar ribbons along curves and three dimensional ribbons as subsets of arbitrary surfaces in  $\mathbb{R}^3$ . The main result shows that the distance between the curvature of the planar curve (the planar design) and the geodesic curvature of the three dimensional supporting curve of the ribbon controls the Green-Lagrange strain tensor, so that the small-strain (but large rotations) assumptions can be fulfilled by an appropriate choice of the planar geometry. The fourth section describes a specific application: fabrication of a partial cover of the sphere from a planar pre-stressed bilayer material by using a design based on the geodesic curvature of constant-latitude circles.

## 1.2 Geometric and kinematical settings

Let us consider a plate with mid-surface  $R_0 \subset \mathbb{R}^2$  and thickness  $H = H(\bar{X})$  in the Lagrangian configuration (here  $\bar{X} = (X_1, X_2)$ ) and let  $S_0 \subset \mathbb{R}^3$  be the mid-surface of an Eulerian shell of thickness  $h$ , with  $e_3$  the unit normal and  $\mathcal{K}$  the curvature tensor acting from the tangent plane into itself.

In what follows,  $\delta \ll 1$  will be a small parameter characterizing the Eulerian and Lagrangian shell thickness and such that :

$$h|\mathcal{K}| = \mathcal{O}(\delta), \quad H/L_c = \mathcal{O}(\delta), \quad |\nabla_2 H| = \mathcal{O}(\delta), \quad (1.1)$$

where  $L_c$  is the characteristic length of the surface and  $\nabla_2$  is the gradient with respect to  $\bar{X} \in R_0$ .

The main geometric assumption in Danescu and Ionescu (2020) is that there exists a transformation  $\mathbf{x} : R_0 \rightarrow S_0$  of the Lagrangian mid-surface  $R_0$  into the designed Eulerian one  $S_0$  such that the associated deformation of the geometric transformation is small, i.e.,

$$|\mathbf{E}_2| = \frac{1}{2} |\nabla_2^T \mathbf{x} \nabla_2 \mathbf{x} - \mathbf{I}_2| = \mathcal{O}(\delta). \quad (1.2)$$

Here  $\mathbf{I}_2 = \mathbf{c}_1 \otimes \mathbf{c}_1 + \mathbf{c}_2 \otimes \mathbf{c}_2$  is the identity tensor on  $\mathbb{R}^2$  and  $\{\mathbf{c}_1, \mathbf{c}_2, \mathbf{c}_3\}$  is the Cartesian basis in the Lagrangian description and hereafter we denote by  $\mathbf{K} = \nabla_2^T \mathbf{x} \mathcal{K} \nabla_2 \mathbf{x}$  the Lagrangian curvature tensor acting from  $\mathbb{R}^2$  into itself.

The kinematics of the plate deformation considered in Danescu and Ionescu (2020) involves the classical Love-Kirchhoff assumption, i.e.: *the normal to the plate mid-plane remains normal to the designed mid-surface* but in a finite deformation context and thus including large rotations. In addition, the transversal deformation is affine with respect to the plate thickness. Superposed to the kinematics associated to the exact design which reproduces the target mid-surface, we consider a small perturbation of Love-Kirchhoff type in order to compensate the small (membrane) deformation of the proposed geometric transformation. As a consequence, the mid-surface of this overall kinematics will be close to the designed mid-surface, and for this reason we called it *approximate design kinematics*.

### 1.3 Weak transversal homogeneity and the moment equations

Although, the general theory developed in Danescu and Ionescu (2020) can cover the general anisotropic framework, here we restrict to cubic materials since our designed experiment involve multilayered cubic III-V semiconductor alloy  $\text{In}_{1-\alpha}\text{Ga}_\alpha\text{P}$  for  $\alpha$  small. In order to account for small-strains but large rotations including inhomogeneous pre-stress we consider a linear constitutive relation between the second Piola-Kirchhoff stress  $\mathbf{S}$  tensor and the Green strain-tensor  $\mathbf{E} = \frac{1}{2}(\mathbf{F}^T\mathbf{F} - \mathbf{I})$  in the form

$$\mathbf{S} = \mathbb{C}(X_3)[\mathbf{E}] + \mathbf{S}^*(X_3) + \Sigma\mathcal{O}(\delta^2), \quad (1.3)$$

where  $\Sigma$  is a characteristic stress and both the material parameters  $\mathbb{C} = (C_{ij})$  (Voigt notation) and the pre-stress  $\mathbf{S}^*$  depends on the normal coordinate in the reference configuration. Moreover, following Danescu and Ionescu (2021) we assume that the elasticities  $\mathbb{C}$  obey the *weak transversal heterogeneity* condition, i.e.,

$$\langle C_{ij} \rangle_2 = \Sigma\mathcal{O}(\delta), \quad \langle C_{ij} \rangle_3 = \frac{1}{12}\langle C_{ij} \rangle_1 + \Sigma\mathcal{O}(\delta), \quad (1.4)$$

where the successive averages (moments) of a  $X_3$ -dependent function  $\langle f \rangle_n$  ( $n = 1, 2, 3$ ) are defined through

$$\langle f \rangle_n = \frac{1}{H^n} \int_{-H/2}^{H/2} X_3^{n-1} f(X_3) dX_3. \quad (1.5)$$

Taking into account that during the MBE growth the upper surface of the multi-layer structure is stress-free, we assume that the pre-stress acting surfaces parallel to the mid-surface vanishes, so that  $\mathbf{S}^* \mathbf{e}_3 = \mathbf{0}$ . Then, following Danescu and Ionescu (2020), the moments equations are

$$\text{div}\left(\frac{H}{12}\mathbb{M}[\mathbf{K}] + \langle \mathbf{S}_2^* \rangle_2\right) = \mathbf{0} \text{ in } R_0, \quad \left(\frac{H}{12}\mathbb{M}[\mathbf{K}] + \langle \mathbf{S}_2^* \rangle_2\right)\nu_{ext} = \mathbf{0} \text{ on } \partial R_0, \quad (1.6)$$

$$\left(\frac{H}{12}\mathbb{M}[\mathbf{K}] + \langle \mathbf{S}_2^* \rangle_2\right) : \mathbf{K} = \mathbf{0} \quad \text{in } R_0, \quad (1.7)$$

where  $\mathbf{S}_2^*$  is the in-plane pre-stress and  $\mathbb{M} = \{M_{ij}\}$  is related to the in-plane reduced elasticity, i.e.,

$$\mathbb{M}[\mathbf{A}] = \langle \mathbb{D}_2 \rangle_1[\mathbf{A}] - \frac{\langle C_{12} \rangle_1^2}{\langle C_{11} \rangle_1} (\mathbf{I} : \mathbf{A}) \mathbf{I} \quad (1.8)$$

and  $\mathbb{D}_2$  is the in-plane part of the Voigt tensor.

Obviously, equations (1.6)-(1.7) are satisfied if the pre-stress  $\mathbf{S}^*$  is such that

$$\langle \mathbf{S}_2^* \rangle_2 = -\frac{H}{12}\mathbb{M}[\mathbf{K}]. \quad (1.9)$$

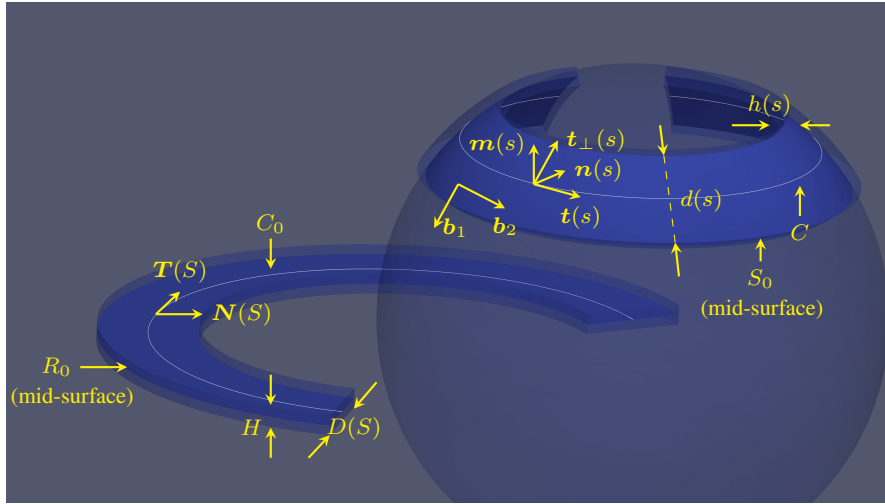


**Fig. 1.1** Geometric elements of the planar ribbon : thickness  $H(S)$ , width  $D(S)$ , the tangent and normal vectors  $(\mathbf{T}(S)$  and  $\mathbf{N}(S))$  along the curve  $C_0$  located in the mid-surface  $R_0$  and the geometric elements for the shell-ribbon with mid-surface  $S_0$  along the curve  $C$ :  $\{\mathbf{t}(s), \mathbf{n}(s), \mathbf{m}(s)\}$  Frenet frame along  $C$ , the vector  $\mathbf{t}_\perp$  (located in the tangent plane to  $S_0$ ), thickness  $h(s)$  and width  $d(s)$ .

## 1.4 Small strain deformation of a ribbon

If  $S \in [0, L]$  and  $\kappa_0(S)$  are the arc-length and the curvature of a planar curve  $C_0$  located at  $\mathbf{R}(S) \in \mathbb{R}^2$  with tangent  $\mathbf{T}(S)$  and normal  $\mathbf{N}(S)$ , we define (see Figure 1.1) the planar ribbon  $R_0 \subset \mathbb{R}^2$  along  $C_0$  of width  $D = D(S)$  as

$$R_0 = \{\mathbf{R}(S) + Q\mathbf{N}(S); S \in (0, L), Q \in (-D(S), D(S))\}. \quad (1.10)$$

Let  $S_0$  denotes the mid-surface of a shell, given by its parametric description  $\mathbf{u} \rightarrow \mathbf{r}_{S_0}(\mathbf{u}) \in \mathbb{R}^3$ , where  $\mathbf{u} = (u_1, u_2)$  are coordinates in some subset  $\Omega \subset \mathbb{R}^2$ . If  $\delta \ll 1$  is a small parameter, our goal is to provide conditions for the existence of a map  $\mathbf{x} : R_0 \rightarrow S_0$  with small strain, i.e. (1.2) holds uniformly with respect to  $\mathbf{X} \in R_0$ .

Let us compute the (Lagrangian) metric tensor of the planar ribbon defined in (1.10). The local basis, associated to the coordinates  $(S, Q)$ , is  $\mathbf{b}_S = \mathbf{T} - Q\kappa_0\mathbf{N}$  and  $\mathbf{b}_Q = \mathbf{N}$  and thus the Lamé coefficients and metric tensor are

$$L_S^2 = g_{SS} = 1 - 2Q\kappa_0 + Q^2\kappa_0^2, \quad g_{SQ} = 0, \quad L_Q^2 = g_{QQ} = 1. \quad (1.11)$$

In order to chose among the multiple ways that map a ribbon on a surface, we study the particular case in which the ribbon cover the shell mid-surface along a given curve  $C \subset S_0$  (see Figure 1.1). As a curve in  $\mathbb{R}^3$ ,  $C$  posses its intrinsic geometric features : arc-length  $s$ , Frenet frame  $(\mathbf{t}(s), \mathbf{n}(s), \mathbf{m}(s))$ , curvature  $\kappa(s)$  and torsion  $\tau(s)$  and, obviously, the tangent plane to the shell mid-surface  $S_0$  contains the tangent vector  $\mathbf{t}(s)$  to  $C$ .

Let  $\mathbf{u}^0(s) = (u_1^0(s), u_2^0(s))$  be the arc-length parametrization of the curve  $C \subset S_0$ . Then,  $\mathbf{t} = \frac{\partial \mathbf{r}}{\partial u_i^0} \frac{du_i^0}{ds} = \mathbf{b}_i \frac{du_i^0}{ds}$  is the description of the tangent vector to  $C$  in the covariant basis  $\{\mathbf{b}_1, \mathbf{b}_2\}$  on  $S_0$ . The main idea is to map the  $q$  coordinates in a neighborhood of the curve  $C \subset S_0$  in the direction  $\mathbf{t}_\perp(s)$ , which is orthogonal to its tangent vector of the curve and belongs to the tangent plane of the surface , i.e.  $\mathbf{t}_\perp(s) = \mathbf{e}_3(\mathbf{u}^0(s)) \wedge \mathbf{t}(s)$ . More precisely, if we put

$$u_i(s, q) = u_i^0(s) + qv_i(s, q), \quad v_i^0(s) = v_i(s, 0), \quad i = 1, 2, \quad (1.12)$$

then the ribbon surface is given by

$$S_0 = \{\mathbf{r}_{S_0}(\mathbf{u}(s, q)); s \in (0, l), q \in (-d(s), d(s))\}, \quad (1.13)$$

where  $d$  is the ribbon width, and from  $\mathbf{t}_\perp(s) = \frac{\partial \mathbf{r}}{\partial q}(s, 0) = \frac{\partial \mathbf{r}}{\partial u_i} \frac{\partial u_i}{\partial q}(s, 0) = \mathbf{b}_i v_i^0(s)$  we get

$$v_i^0(s) = \mathbf{t}_\perp(s) \cdot \mathbf{b}^i(\mathbf{u}^0(s)). \quad (1.14)$$

If the order of magnitude for the ribbons widths with respect to the curvatures of the curves  $C_0$  and  $C$  as well as to the curvature tensor of the surface  $S_0$ , are such that :

$$D(S)\kappa_0(S) = \mathcal{O}(\delta^{1/2}), \quad d(s)|\mathcal{K}(\mathbf{u}^0(s))|, \quad d(s)\kappa(s)(\mathbf{t}_\perp \cdot \mathbf{m}) = \mathcal{O}(\delta^{1/2}), \quad (1.15)$$

then an estimation of the Lagrangian and Eulerian metric tensors at order  $\mathcal{O}(\delta)$  was obtained in Danescu and Ionescu (2021). To see that, let us compute the (Eulerian) metric tensor of the surface  $S_0$  up to first-order with respect to  $q$ . We have successively

$$\begin{aligned}
g_{qq}(s, q) &= g_{ij}(s, q) \frac{\partial u_i}{\partial q} \frac{\partial u_j}{\partial q} = \left( g_{ij}(s, 0) + q \frac{\partial g_{ij}}{\partial q}(s, 0) \right) \frac{\partial u_i}{\partial q} \frac{\partial u_j}{\partial q} + \mathcal{O}(\delta) = \\
&g_{ij}(s, 0) v_i^0 v_j^0 + q \left( 4g_{ij}(s, 0) v_i^0 \frac{\partial v_j}{\partial q}(s, 0) + \frac{\partial g_{ij}}{\partial u_k}(s, 0) v_i^0 v_j^0 v_k^0 \right) + \mathcal{O}(\delta) \\
&= |\mathbf{t}_\perp(s)|^2 + q v_i^0(s) \left( 4g_{ij}(s, 0) \frac{\partial v_j}{\partial q}(s, 0) + \frac{\partial g_{ij}}{\partial u_k}(s, 0) v_j^0(s) v_k^0(s) \right) + \mathcal{O}(\delta),
\end{aligned}$$

and by choosing

$$\frac{\partial v_l}{\partial q}(s, 0) = -\frac{1}{4} g^{li}(s, 0) \frac{\partial g_{ij}}{\partial u_k}(s, 0) v_j^0(s) v_k^0(s), \quad (1.16)$$

we obtain  $g_{qq} = 1 + \mathcal{O}(\delta)$ . Moreover,

$$\begin{aligned}
g_{sq} &= g_{ij} \frac{\partial u_i}{\partial s} \frac{\partial u_j}{\partial q} = \left( g_{ij}(s, 0) + q \frac{\partial g_{ij}}{\partial q}(s, 0) \right) \frac{\partial u_i}{\partial s} \frac{\partial u_j}{\partial q} + \mathcal{O}(\delta) = \\
&= g_{ij}(s, 0) \frac{du_i^0}{ds} v_j^0 + q \left( g_{ij}(s, 0) \frac{dv_i^0}{ds} v_j^0 + 2g_{ij}(s, 0) \frac{du_i^0}{ds} \frac{\partial v_j}{\partial q}(s, 0) + \right. \\
&\quad \left. + \frac{\partial g_{ij}}{\partial u_k}(s, 0) v_k^0 \frac{du_i^0}{ds} v_j^0 \right) + \mathcal{O}(\delta)
\end{aligned}$$

and, since  $g_{ij}(s, 0) \frac{du_i^0}{ds} v_j^0 = \mathbf{t} \cdot \mathbf{t}_\perp = 0$ , using (1.16) we obtain

$$\begin{aligned}
g_{sq} &= \frac{q}{2} \left( 2g_{ij}(s, 0) \frac{dv_i^0}{ds} v_j^0 + \frac{\partial g_{ij}}{\partial u_k}(s, 0) \frac{du_i^0}{ds} v_k^0 v_j^0 \right) + \mathcal{O}(\delta) = \\
&= \frac{q}{2} \frac{d}{ds} (\mathbf{t}_\perp \cdot \mathbf{t}_\perp) + \mathcal{O}(\delta).
\end{aligned}$$

Finally,

$$\begin{aligned}
g_{ss}(s, q) &= \left( g_{ij}(s, 0) + q \frac{\partial g_{ij}}{\partial u_k} \frac{\partial u_k}{\partial q} \right) \frac{\partial u_i}{\partial s} \frac{\partial u_j}{\partial s} + \mathcal{O}(\delta) = g_{ij}(s, 0) \frac{du_i^0}{ds} \frac{du_j^0}{ds} + \\
&+ q \left( 2g_{ij}(s, 0) \frac{du_i^0}{ds} \frac{dv_j^0}{ds} + \frac{\partial g_{ij}}{\partial u_k}(s, 0) v_k^0 \frac{du_i^0}{ds} \frac{du_j^0}{ds} \right) + \mathcal{O}(\delta) = \\
&= |\mathbf{t}(s)|^2 + 2q \left( \frac{d\mathbf{t}_\perp}{ds} \cdot \mathbf{t} \right) + \mathcal{O}(\delta) = 1 + 2q \left( \frac{d\mathbf{t}_\perp}{ds} \cdot \mathbf{t} \right) + \mathcal{O}(\delta).
\end{aligned}$$

But, since  $\mathbf{t}_\perp \cdot \mathbf{t} = 0$  we have  $\mathbf{t}_\perp = (\mathbf{t}_\perp \cdot \mathbf{n})\mathbf{n} + (\mathbf{t}_\perp \cdot \mathbf{m})\mathbf{m}$  so that, using the Frenet formulae, we obtain

$$\frac{d\mathbf{t}_\perp}{ds} \cdot \mathbf{t} = -\frac{d\mathbf{t}}{ds} \cdot \mathbf{t}_\perp = -\kappa(\mathbf{t}_\perp \cdot \mathbf{m}). \quad (1.17)$$

This last result emphasize the role played by the *geodesic curvature*  $\kappa^{geo} = \kappa(\mathbf{t}_\perp \cdot \mathbf{m})$ , which is the projection of the curvature of  $C$  into the tangent plane of the manifold



$S_0$ , in the estimation of the metric tensor. To summarize, we obtained :

$$g_{ss} = 1 - 2q\kappa(s)\mathbf{t}_\perp \cdot \mathbf{m} + \mathcal{O}(\delta), \quad g_{sq} = \mathcal{O}(\delta), \quad g_{qq} = 1 + \mathcal{O}(\delta), \quad (1.18)$$

$$g_{SS} = 1 - 2Q\kappa^0(S) + \mathcal{O}(\delta), \quad g_{SQ} = 0, \quad g_{QQ} = 1 + \mathcal{O}(\delta). \quad (1.19)$$

By using  $(s, q) = (S, Q) \in (0, L) \times (-D, D)$ , we are now able to estimate the Green-Lagrange strain tensor of the map  $\mathbf{x} : R_0 \rightarrow S_0$ . Since the gradient tensor  $\mathbf{F}$  can be written as  $\mathbf{F} = \mathbf{b}_s \otimes \mathbf{b}^S + \mathbf{b}_q \otimes \mathbf{b}^Q$ , taking into account (1.19) and (1.18), we obtain

$$\mathbf{F}^T \mathbf{F} = L_s^2 \mathbf{b}_S \otimes \mathbf{b}_S + \mathbf{b}_Q \otimes \mathbf{b}_Q + \mathcal{O}(\delta) = \mathbf{I} - (1 - g_{ss}/g_{SS})\mathbf{e}_S \otimes \mathbf{e}_S + \mathcal{O}(\delta)$$

and thus

$$\begin{aligned} \mathbf{E}_2 &= \frac{1}{2} \left( \frac{g_{ss}}{g_{SS}} - 1 \right) \mathbf{e}_S \otimes \mathbf{e}_S + \mathcal{O}(\delta) = \\ &= Q[\kappa_0(S) - \kappa(S)(\mathbf{t}_\perp \cdot \mathbf{m})] \mathbf{e}_S \otimes \mathbf{e}_S + \mathcal{O}(\delta). \end{aligned} \quad (1.20)$$

We conclude that by choosing the curvature of the planar curve  $C_0$  equal to the geodesic curvature of the supporting curve of the shell-ribbon  $C \subset S_0$  the Green-Lagrange tensor is small, i.e.

$$\text{if } \kappa_0 = \kappa^{geo} = \kappa \mathbf{t}_\perp \cdot \mathbf{m}, \quad \text{then } \mathbf{E} = \mathcal{O}(\delta). \quad (1.21)$$

## 1.5 From theory to fabrication of a nano-sphere

Let  $(r, \theta, \phi)$  be the spherical coordinates in  $\mathbb{R}^3$  and denote by  $\mathbf{e}_r = \mathbf{e}_r(\theta, \phi)$ ,  $\mathbf{e}_\theta = \mathbf{e}_\theta(\theta, \phi)$ ,  $\mathbf{e}_\phi = \mathbf{e}_\phi(\phi)$  the local physical basis. Let  $S_0$  denote the surface of the sphere of radius  $R_*$  with Lamé coefficients  $L_\theta = R_*$ ,  $L_\phi = R_* \sin(\theta)$  and the unit normal  $\mathbf{e}_3(\theta, \phi) = \mathbf{e}_r(\theta, \phi)$ . Then, the curvature tensor on  $S_0$  is

$$\mathcal{K} = -\frac{1}{R_*} (\mathbf{e}_\theta \otimes \mathbf{e}_\theta + \mathbf{e}_\phi \otimes \mathbf{e}_\phi).$$

Let  $C \subset S_0$  be a given curve with arc-length  $s$ , parametric description  $s \rightarrow (\theta^0(s), \phi^0(s))$  and geodesic curvature  $\kappa^{geo}(s)$ . If  $C_0$  is the planar curve with curvature  $\kappa_0(s) = \kappa^{geo}(s)$  and  $R_0$  is the planar ribbon along  $C_0$  (see definition (1.10)) with the width  $d(s)$  such that (1.15) holds then, from the small-strain membrane condition (1.2) we get

$$\mathbf{K} = \frac{1}{R_*} (\mathbf{I}_2 + \mathcal{O}(\delta)).$$

From the plate-to shell model we find that a shell-ribbon  $S_0$  of a spherical shell of radius  $R_*$  along the curve  $C$ , could be designed from a planar ribbon  $R_0$  along a curve  $C_0$  if (1.21) holds. The pre-stress momentum have to be designed such that

$\langle \mathbf{S}_2^* \rangle_2 = -\frac{H^3}{12R_*} \mathbb{M}[\mathbf{I}_2]$  and can be obtained with an isotropic and homogeneous pre-stress, i.e.,  $\mathbf{S}_2^* = \sigma^* \mathbf{I}_2$ , where

$$\langle \sigma^* \rangle_2 = \frac{H}{12R_*} \frac{\langle C_{11}^2 \rangle_1 + \langle C_{12} \rangle_1 \langle C_{11} \rangle_1 - 2\langle C_{12} \rangle_1^2}{\langle C_{11} \rangle_1}. \quad (1.22)$$

### 1.5.1 Optimal covering with constant parallel ribbons

For constant latitude curves, i.e.,  $\theta(s) = \theta^0$ , we have  $\phi^0 = s/(R_* \sin(\theta_0))$  so that  $d/R_* = \mathcal{O}(\delta^{1/2})$ ,  $d \cot(\theta^0)/R_* = \mathcal{O}(\delta^{1/2})$  and the geodesic curvature is  $\kappa_0 = \kappa^{geo} = \cot(\theta^0)/R_*$ . This means that the width of successive ribbons will decrease with the latitude. As a straightforward consequence, the fit of successive positions and widths of constant latitude ribbons for a complete cover of the sphere is a nontrivial problem. We recall here a result from Danescu and Ionescu (2021) concerning a semi-analytical optimal covering of the sphere.

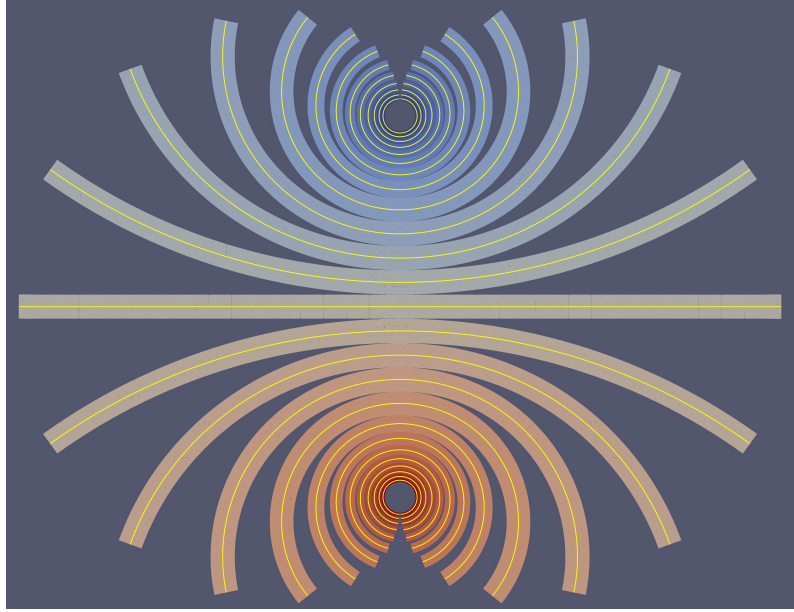


**Fig. 1.2** An optimal covering of the sphere with constant latitude ribbons obtained by implementing the solutions of recursive system (1.24) for  $\delta = 10^{-2}$ .

If  $\theta_k$  denote the latitudes of the supporting curve for successive ribbons then, for the  $k^{\text{th}}$  ribbon, the arc-length is such that  $s \in (-\pi R_* \cos \theta_k, \pi R_* \cos \theta_k)$  and the angular variable  $\theta(q) = \pi/2 - \theta_k - q/R_*$  for  $q \in (-d_k, d_k)$ . A symmetric solution

can be obtained as follows : take  $\theta_0 = 0$ ,  $\theta_k = -\theta_k$  and notice that the covering condition and (1.15) can be expressed as

$$d_k \leq \delta^{1/2} R_* \min(1, \cot \theta_k), \quad R_*(\theta_{k+1} - \theta_k) = d_k + d_{k+1}. \quad (1.23)$$

It follows that for  $\theta < \pi/4$  we can consider constant width ribbons with  $\theta_k = 2k\delta^{1/2}$  and thus  $d_k = \delta^{1/2} R_*$  for  $|k| \leq \lfloor \frac{\pi}{8\sqrt{\delta}} - \frac{1}{2} \rfloor$  (here  $[x]$  is the entire part of  $x$ ) while for  $k > \lfloor \frac{\pi}{8\sqrt{\delta}} - \frac{1}{2} \rfloor$  we have to solve recursively the nonlinear equation

$$x - \delta^{1/2} \cot x = \theta_k + \frac{d_k}{R_*}, \quad (1.24)$$

whose solution  $\theta_{k+1}$  provide

$$d_{k+1} = R_*(\theta_{k+1} - \theta_k). \quad (1.25)$$

An implementation of this procedure for  $\delta = 10^{-2}$  provide the design illustrated in Figure 1.2.

### 1.5.2 Elastic layers with pre-stress : material parameters

The experimental implementation of the sphere covering with variable width ribbons, presented in the previous subsection, is difficult due to very sharp angles between successive ribbons near the vertical symmetry axis, and thus incompatible with the spatial resolution of the photo-lithography processes. However, in order to illustrate the role of the geodesic curvature in the design problem we focus here on the partial cover of the sphere with constant latitude ribbons.

Since the planar design is dependent on the target surface curvature we start by the epitaxial growth of the bi-layer semiconductor structure : a 60 nm thick  $\text{In}_{0.88}\text{Ga}_{0.12}\text{P}$  layer (further denoted InGaP) grown on a 145 nm thick InP layer. The bi-layer was grown on an InP substrate previously covered by a 500 nm thick InGaAs sacrificial layer. Using data from the litterature, we have :

$$\begin{aligned} C_{11}^{\text{InP}} &= 101.1 \text{ GPa}, & C_{11}^{\text{InGaP}} &= 105.8 \text{ GPa}, \\ C_{12}^{\text{InP}} &= 56.1 \text{ GPa}, & C_{12}^{\text{InGaP}} &= 56.8 \text{ GPa}, \\ C_{44}^{\text{InP}} &= 45.6 \text{ GPa}, & C_{44}^{\text{InGaP}} &= 48.5 \text{ GPa}, \end{aligned} \quad (1.26)$$

so that the characteristic stress  $\Sigma = 100$  GPa. For  $\delta = 10^{-2}$  we verify that indeed

$$\langle C_{ij} \rangle_2 = \Sigma \mathcal{O}(\delta), \quad \langle C_{ij} \rangle_3 - \frac{1}{12} \langle C_{ij} \rangle_1 = \Sigma \mathcal{O}(\delta), \quad (1.27)$$

so that the assumption of weak transversal homogeneity is fulfilled. The lattice parameters for the InP and InGaP layers are respectively

$$a_{\text{InP}} = 5.8687 \text{ \AA}, \quad a_{\text{In}_{0.88}\text{Ga}_{0.12}\text{P}} = 5.8185 \text{ \AA}, \quad (1.28)$$

and correspond to a spherical pre-strain (extension) in the upper layer of  $m = \text{diag}(0.86\%, 0.868\%)$ . For practical applications, it is the fraction of Ga in the upper layer ( $\text{In}_\alpha\text{Ga}_{1-\alpha}\text{As}$ ) which has to be fixed as a function of the radius of the target sphere, but for simplicity here we use the equation (1.9) in order to compute the radius of the object that can be obtained at  $\alpha = 0.12$ .

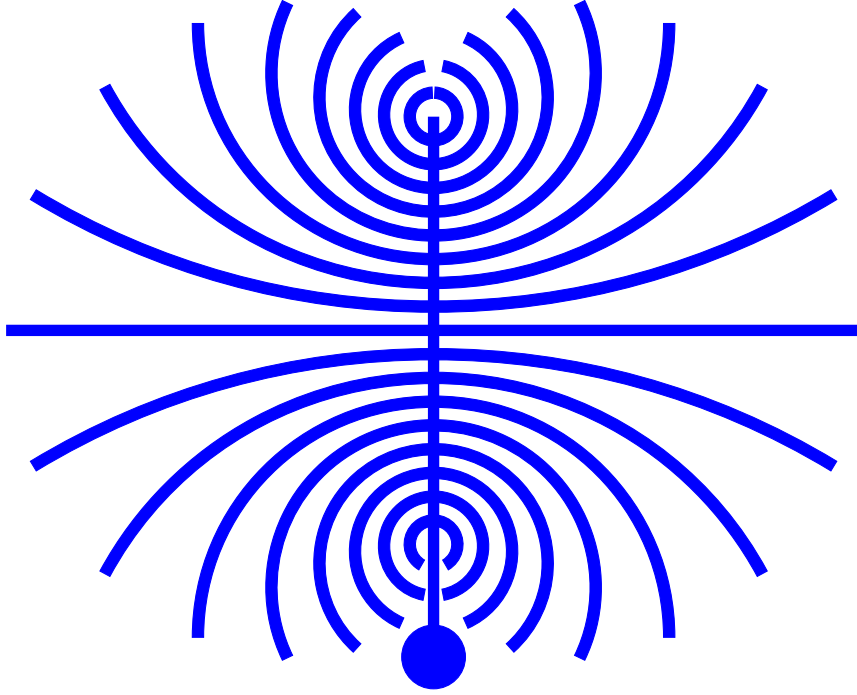


**Fig. 1.3** The planar grid designed to cover the sphere. The horizontal straight line will fully cover the equator while the lower and upper parts will cover the North and South hemispheres, respectively. Notice the slight modification of the length for small arcs near the South pole needed in order to keep the relaxed structure attached through the filled round dot (with a characteristic size larger than the lateral dimensions of the curved ribbons) to the substrate during the under-etching process.

### 1.5.3 Design and fabrication

In order to cover the sphere of radius  $R_*$  with constant latitude ribbons we notice that the radius of the ribbon at latitude  $\theta$  is  $R_* \cos \theta$  and their geodesic curvature, which is exactly the inverse of the planar design radius, is constant and equal to

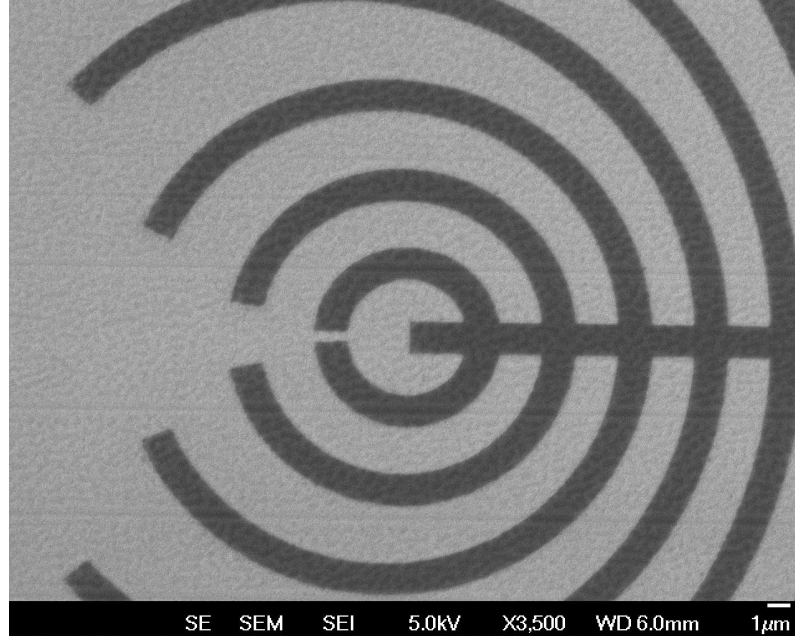


**Fig. 1.4** SEM image of the sample after the development process before the reactive ion etching (RIE).

$\kappa(\theta) = \frac{1}{R^*} \tan \theta$ . For simplicity, we chose the width of all ribbons equal to  $1.5 \mu\text{m}$  (for visual comfort, the actual scale in Figure 1.3 is not the same as the implemented design in 1.5) and design a geodesic half-circle to ensure connectivity between the constant latitude ribbons. Using the intersection of the two straight lines in figure 1.3 as the origin of the coordinate system in the plane, positions of the 8 pairs of symmetric arcs corresponding to constant latitude arcs located at  $\pm \frac{n\pi}{18}$  ( $n = 1, \dots, 8$ ) in the North and South hemi-sphere. Their corresponding centers radii and angular extensions are

$$C_n^\pm = \left(0, \pm R \left( \frac{n\pi}{18} + \frac{1}{\tan \theta} \right)\right), \quad R_n = R / \tan \theta, \quad \theta_n = \pi \sin\left(\frac{n\pi}{18}\right). \quad (1.29)$$

Fabrication of the design illustrated in Figure 1.3 involve several steps : we start by the deposition of a 90 nm thick  $\text{SiO}_2$  hard mask followed by the deposition of a 130 nm thick negative resist film (AR-N7520.07). Next step is electron beam lithography performed by using a modified SEM (FEI Inspect F) and the RAITH Elphy Quantum software. The result after the development of the lithographic process is illustrated in Figure 1.4. The reactive ion etching (RIE) is then performed in order to transfer the pattern into the silica mask and then into the multilayer structure. The result of this process is represented in Figures 1.5 (both optical microscope and SEM images). At this step, the structure is still attached on the sacrificial layer but the

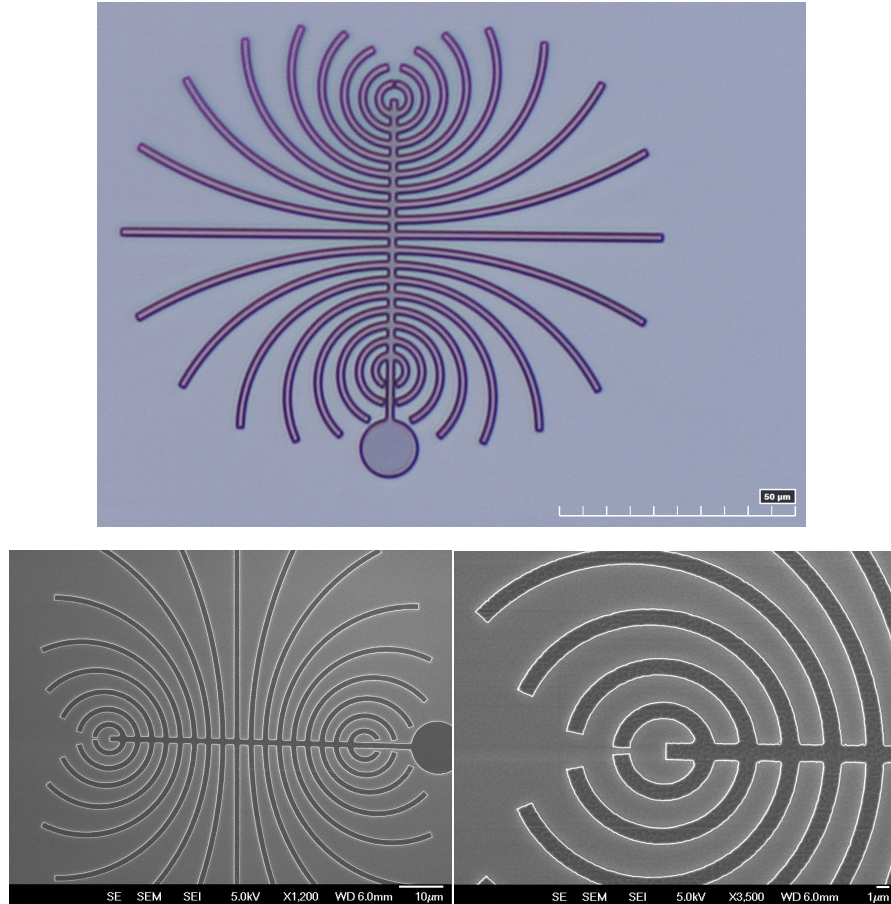


**Fig. 1.5** Optical microscope view of the structure obtained after etching the multilayer material, still maintained attached to the substrate by the sacrificial layer.

lateral relaxation of the pre-stress in the bilayer material takes place. Despite the small width ( $1.5 \mu\text{m}$ ) and the ultra-small thickness (205 nm) the axial pre-stress is still present in the structure and will be released only during the process of under-etching of the sacrificial layer. In order to keep the relaxed structure attached to the substrate the radius of the attachment circle (designed in the lower part of Figure 1.3) have to be slightly larger than the width of various arcs of the design.

Next, the under-etching is performed using diluted  $\text{FeCl}_3$  to selectively remove the InGaAs sacrificial layer so as to release the pre-stress in the multilayer. Successive  $\text{H}_2\text{O}$ , acetone and methanol rising baths were performed before a  $\text{CO}_2$  supercritical drying step, needed in order to circumvent the mechanical actions induced by the surface tension at liquid/solid interfaces. As expected, the fully relaxed structure covers the surface of the sphere with constant latitude ribbons, with only small

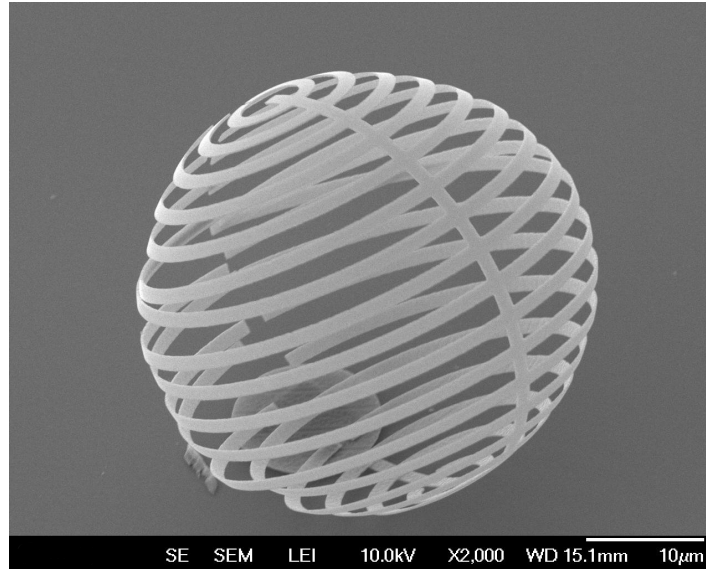


**Fig. 1.6** The relaxed shape confirms that the geodesic curvature design relax as expected into constant latitude circles on the sphere.

alignment defects at the ends. Obviously, a large variety of different designs can be implemented but, as already stated, technological limitations associated with the photolithographic process (sharp angles) do not allow all of these designs to be successfully implemented.

## 1.6 Conclusions and perspectives

The fabrication of nano-shells, is in itself a technological challenge as it encompasses the traditional planar technology. One way to obtain such structures is to release the pre-stressed nano-plates, fabricated by layer-by-layer deposition, to obtain a target shell geometry. The presence of several geometrical and technological restrictions can be circumvented by the use of three-dimensional thin ribbons in order to cover a desired surface. The geodesic curvature plays a fundamental role for the design of both the geometry of ribbons that cover arbitrary surfaces starting from planar structures and the pre-stress needed to obtain them. The main result shows that, for multilayered structures with weak-transversal homogeneity, if the curvature of the planar ribbon is equal to the geodesic curvature of the supporting curve then there exists a pre-stress such that a small-width and small-thickness planar ribbon relaxes toward a 3D ribbon covering the surface along the supporting curve. We illustrate our theoretical results by the design and fabrication of a partial cover of the sphere with constant-latitude ribbons starting from a planar design containing arcs with constant

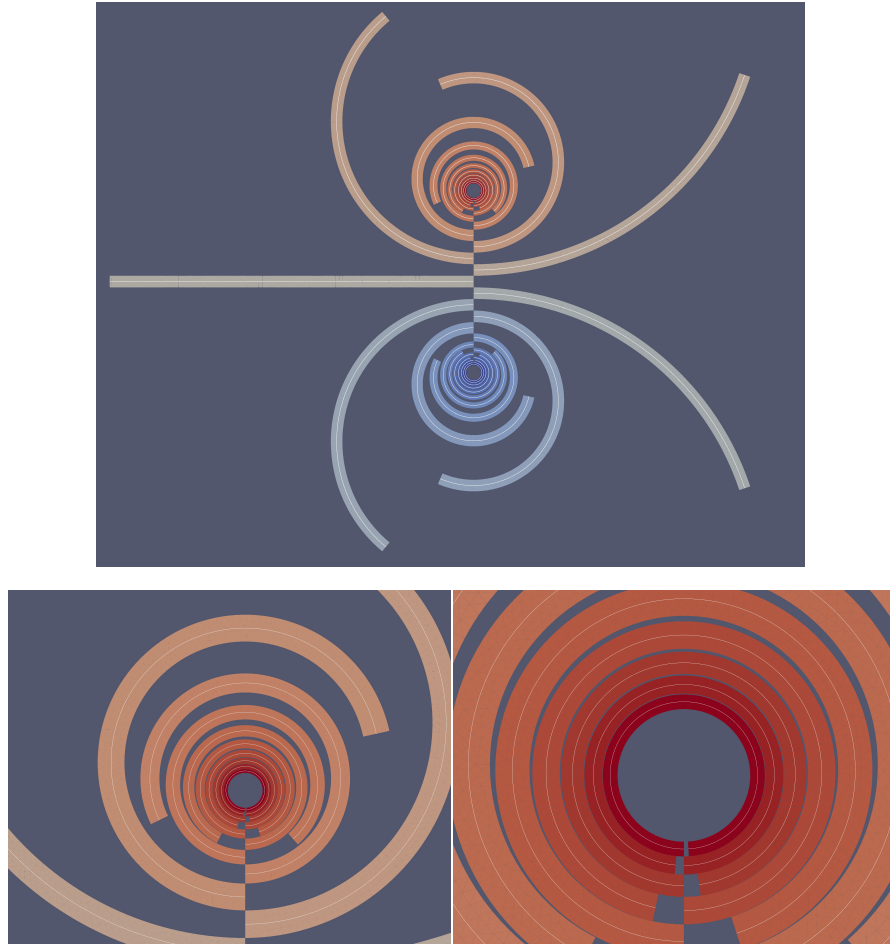


**Fig. 1.7** Top: Optimal covering of the sphere for  $\delta = 10^{-2}$ . Alternative distribution of the constant latitude arcs on the left (respectively right) part of the initial design present in Figure 1.2 to avoid sharp angles along the vertical symmetry axis. Bottom: zoom on the central zone.

curvature and a bilayer semi-conductor bilayer material with controlled composition ( $\text{In}_{0.88}\text{Ga}_{0.12}\text{P}/\text{InP}$ ).

Extensions of these results to obtain a complete cover of the sphere are limited by the resolution of the lithographic process, difficult to implement at very sharp angles. A solution to overcome this technological drawback of the (sharp angles) lithographic process is illustrated in Figure 1.7. Here, in order to avoid the sharp angles between successive ribbons located at constant latitude we chose to design alternative left and right constant radius arcs corresponding to successive constant latitude ribbons. The ideal picture in Figure 1.7 does not include a small vertical segment, which is needed in order to attach the constant curvature arcs to the structure. In fact, the



design in Figure 1.7 contains exactly the same arcs as that of the Figure 1.2 but their positions are such that sharp angles along the vertical symmetry line in Figure 1.2 are avoided. However, a closer look to the design in Figure 1.7, reveals very small distances between successive ribbons (also present in the initial design in Figure 1.2 between large latitude ribbons).

The general results in Danescu and Ionescu (2021) provide solutions to both partial and total covers of other non-developable (orientable or not) three-dimensional surfaces as the torus and the Mobius ribbon, extending the classical setting of isometric transformations. We mention here two interesting extensions: the first one concerns the class of arbitrary transversal homogeneities (and not only weak transversal homogeneities) in which case one has to adapt the general setting in Danescu and Ionescu (2020). The second perspective concerns the fabrication of more complex geometries which require not only bending but also torsion, a problem already discussed in Danescu and Ionescu (2021) which is dependent to more complex (not only hydrostatic) pre-stress. Controlled spatial modulation of the pre-stress, and in particular including controlled shear still remains a technological landmark at the nano-scale.

## References

- de Benito Delgado M, Schmidt B (2020) Energy minimising configurations of pre-strained multilayers. *Journal of Elasticity* 140:1–33
- Ciarlet PG, Mardare C (2018) A nonlinear shell model of koiter’s type. *Comptes Rendus Mathématique* 356(2):227–234
- Danescu A, Ionescu IR (2020) Shell design from planar pre-stressed structures. *Mathematics and Mechanics of Solids* 25(6):1247–1266, DOI 10.1177/1081286520901553
- Danescu A, Ionescu IR (2021) Non-developable shell-strips design from pre-stressed plate-strip. submitted, ArXiv preprint
- Danescu A, Chevalier C, Grenet G, Regreny P, Letartre X, Leclercq JL (2013) Spherical curves design for micro-origami using intrinsic stress relaxation. *Applied Physics Letters* 102(12):123,111
- Danescu A, Regreny P, Cremillieu P, Leclercq J (2018) Fabrication of self-rolling geodesic objects and photonic crystal tubes. *Nanotechnology* 29(28):285,301
- de Benito Delgado, Miguel, Schmidt, Bernd (2021) A hierarchy of multilayered plate models. *ESAIM: COCV* 27:S16
- Fosdick R, Fried E (2016) *The mechanics of ribbons and Möbius bands*. Springer
- Friesecke G, James RD, Müller S (2002a) A theorem on geometric rigidity and the derivation of nonlinear plate theory from three-dimensional elasticity. *Communications on Pure and Applied Mathematics: A Journal Issued by the Courant Institute of Mathematical Sciences* 55(11):1461–1506
- Friesecke G, Müller S, James RD (2002b) Rigorous derivation of nonlinear plate theory and geometric rigidity. *Comptes Rendus Mathématique* 334(2):173–178
- Friesecke G, James RD, Müller S (2006) A hierarchy of plate models derived from nonlinear elasticity by gamma-convergence. *Archive for rational mechanics and analysis* 180(2):183–236
- Le Dret H, Raoult A (1995) The nonlinear membrane model as variational limit of nonlinear three-dimensional elasticity. *Journal de mathématiques pures et appliquées* 74(6):549–578
- Lewicka M, Raoult A (2018) Thin structures with imposed metric. *ESAIM: Proceedings and Surveys* 62:79–90

- Prinz VY (2003) A new concept in fabricating building blocks for nanoelectronic and nanomechanic devices. *Microelectronic engineering* 69(2-4):466–475
- Prinz VY, Golod S (2006) Elastic silicon-film-based nanoshells: formation, properties, and applications. *Journal of Applied Mechanics and Technical Physics* 47(6):867–878
- Prinz VY, Seleznev V, Gutakovskiy A, Chehovskiy A, Preobrazhenskii V, Putyato M, Gavrilova T (2000) Free-standing and overgrown ingaas/gaas nanotubes, nanohelices and their arrays. *Physica E: Low-dimensional Systems and Nanostructures* 6(1-4):828–831
- Prinz VY, Grützmacher D, Beyer A, David C, Ketterer B, Deckardt E (2001) A new technique for fabricating three-dimensional micro-and nanostructures of various shapes. *Nanotechnology* 12(4):399
- Prinz VY, Naumova EV, Golod SV, Seleznev VA, Bocharov AA, Kubarev VV (2017) Terahertz metamaterials and systems based on rolled-up 3d elements: designs, technological approaches, and properties. *Scientific reports* 7:43,334
- Seleznev V, Yamaguchi H, Hirayama Y, Prinz V (2003) Single-turn GaAs/InAs nanotubes fabricated using the supercritical CO<sub>2</sub> drying technique. *Japanese journal of applied physics* 42(7A):L791
- Steigmann DJ (2007a) Asymptotic finite-strain thin-plate theory for elastic solids. *Computers & Mathematics with Applications* 53(2):287–295
- Steigmann DJ (2007b) Thin-plate theory for large elastic deformations. *International Journal of Non-Linear Mechanics* 42(2):233–240
- Steigmann DJ (2013) Koiter shell theory from the perspective of three-dimensional nonlinear elasticity. *Journal of Elasticity* 111(1):91–107
- Steigmann DJ, Ogden RW (2014) Classical plate buckling theory as the small-thickness limit of three-dimensional incremental elasticity. *ZAMM-Journal of Applied Mathematics and Mechanics/Zeitschrift für Angewandte Mathematik und Mechanik* 94(1-2):7–20
- Wang FF, Steigmann DJ, Dai HH (2019) On a uniformly-valid asymptotic plate theory. *International Journal of Non-Linear Mechanics* 112:117–125